Metal assisted chemical etching of silicon and solution synthesis of Cu_2O/Si radial nanowire array heterojunctions

© L. Chetibi, D. Hamana, S. Achour

Laboratory of Advanced Materials Technology,
Ecole Nationale Polytechnique de Constantine and Phases transformations Laboratory,
University of Constantine 1, Algeria

E-mail: d_hamana@yahoo.fr

Received March 15, 2022
Revised March 10, 2023
Accepted for publication March 10, 2023

Cu_2O/Si radial nanowire (NWs) array heterojunctions were prepared by depositing Cu_2O nanoparticles via chemical bath deposition on *n*-Si nanowire arrays that were fabricated by metal-assisted electroless etching. After 20 cycles of deposition, large numbers of Cu_2O nanoparticles with form shells that wrap the upper segment of each Si nanowire. This method of etching offers exceptional simplicity, flexibility, environmental friendliness, and scalability for the fabrication of three-dimensional silicon nanostructures with considerable depths, because of replacement of harsh oxidants such as H_2O_2 and $AgNO_3$.

Keywords: Cu_2O/Si NWs heterojunctions, Cu_2O nanoparticles, metal-assisted electroless etching.

DOI: 10.21883/SC.2023.02.55956.3390

1. Introduction

One-dimensional semiconductor heterojunctions (HJs) are receiving significant research interest due to their application in optoelectronic and electronic devices [1,2]. As one of the fundamental building blocks of nano-optoelectronic devices, Si nanowires (NWs) have been studied intensively, and various HJs based on Si NWs have been demonstrated [3]. Among these HJs, Si NW-based core-shell HJs have attracted much attention for their potential use in photovoltaic, photocatalyst and sensing applications, due to their superior carrier collection capability [4–6]. Because of their excellent light antireflection properties, vertically arrayed Si NWs usually serve as cores in core-shell HJs to obtain efficient light harvesting in optoelectronic devices [7–10]. Cu_2O is one of the relatively less p-type metal oxide semiconductors with a band gap of 2.17 eV [11], and it is a promising material for solar energy conversion and nanoelectronic applications [12,13]. However, as photodetectors (PDs), these pn HJs can only work in the ultraviolet or visible region due to the band gaps for these metal oxides.

One method of fabricating nanostructured Si is metal assisted chemical (MAC) etching which creates Si nanowires (NWs) from a top-down process on a Si piece. The NWs formed by MAC etching depend on parameters such as the orientation of the Si, the doping density of the Si and the etching conditions under which the NWs are formed [14] The large-scale and high-quality aligned Cu_2O nanowires fabricated uniformly on the SiO_2/Si substrate are studied in this paper by the Chemical Bath Deposition (CBD). The CBD method provides simple, time-saving, economic, and environmentally friendly performance in Cu_2O nanowires fabrication even without the help of any templates and catalysts [15]. The novel process and obtained results are verified using Atomic Force Microscope (AFM), Raman Spectroscopy, UV-Visible Spectroscopy and Photo-electrochimical of samples.

Chemical bath deposition (CBD) has widely been used to deposit compound semiconducting thin films because of its low cost, low temperature processing, and suitability for the fabrication of large area devices [16–18]. The controlled formation of porosity and roughness in Si [19–21] has attracted substantial attention, and nanoscale Si in the form of nanocrystals [22], NWs, and mesoporous analogues have been successfully applied [23] to LIBs [24], photovoltaic [25], sensing [26].

Thus, in this paper we search to obtain an heterojunction $p-n$ by a simple methods with lot of performance and proprieties existence in the recent application especially in optic field.

2. Experiments

2.1. Synthesis of Si NW arrays and Cu_2O/Si radial NW arrays

Si NW arrays were prepared using an Ag-assisted electroless etching method on commercially obtained heavily doped *n*-Si (111) wafers. First, piece of Si was immersed in solution of Acetone for cleaning from the dust and print finger, then cleaned with deionized water. After that, it was immersed in a 5% HF aqueous solution for 10 min to make its surface H-terminated. Then, the Si wafer was immediately immersed in a solution composed of 4.8 M HF and 25 mM $AgNO_3$ for 7 min. After washing with deionized water to remove the excess Ag^+ ions, the surface of the Si wafer was covered by a layer of uniform

Ag NPs. Then the Ag NP coated Si piece was placed in an etching solution composed of 4.8 M HF and 0.06 M H_2O_2 for 15 h and 30 min under dark ambient conditions, followed by a thorough rinse with deionized water. Subsequently, dilute aqueous HNO_3 (HNO_3(65–68%)/H_2O = 1 : 1, V/V) was used to dissolve the Ag NPs on the resultant Si pieces. At this point, vertically arrayed Si NW swere formed on the Si substrates. Finally, the resultant piece was again washed with 5% HF to remove the oxide layer then cleaned with deionized water before being dried with heating plate for 1 h.

The resultant pieces of Si NW arrays were then used as the substrates for depositing Cu_2O through a CBD process. The preparation procedures are described as follows. The fresh Si NW arrays were sequentially immersed in two beakers of solution, referred to solutions A and B in this text. Each immersion time was controlled at 20 s. The resultant samples were then rinsed with deionized water. This represents a single cycle of deposition. As the number of deposition cycles increased, the color of the samples gradually changed from black, which is the original color of Si NW arrays, to brown. Solution A was made by adding 50 ml of 1 M $CuSO_4$ to 200 ml of 1 M $Na_2S_2O_3$. Solution B was 500 ml of 1 M NaOH kept in a water bath at 70°C. It should be noted that CTAB ($C_{19}H_{42}BrN$) was absent in our experience. Finally, the samples were dried in ambient temperature, then annealed 1 h at 200°C under vacuum.

2.2. Structural characterization

The surface morphology of the Si NWs before and after the deposition of Cu_2O NPs was characterized by an Atomic Force Microscope (AFM). The composition of samples was analyzed using Raman spectroscopy (Raman spectroscopy Sentrra Bruker), the band gap of copper oxide was measured by UV-Visible spectroscopy (diffuse reflectance in a spectrophotometer JASCO ILN-725-V-676).

2.3. Device fabrication and photoelectric measurements

The PEC measurements were performed with a Solarton analytical SI 1287 electrochemical workstation connected to a three electrode cell system. The working electrode consisted of the prepared sample (Cu_2O NWs) while the counter and reference electrodes consisted of a Pt wire coil and SCE respectively. The PEC was conducted in 1.0 M NaOH aqueous solution under power AM 1.5 illumination of 100 mW/cm^2.

3. Results and discussion

The area of MAC etching has recently been reviewed by Huang et al. [27] and Li [28] showing the vast interest that this subject attracts. The Si NWs produced can be tuned in length from many hundred nanometers to several tens

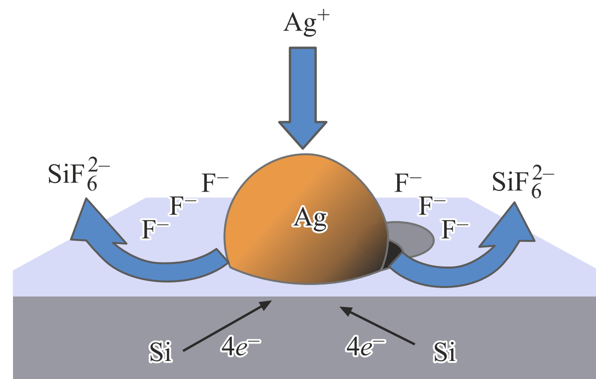

Figure 1. A schematic of the electroless metal deposition process.

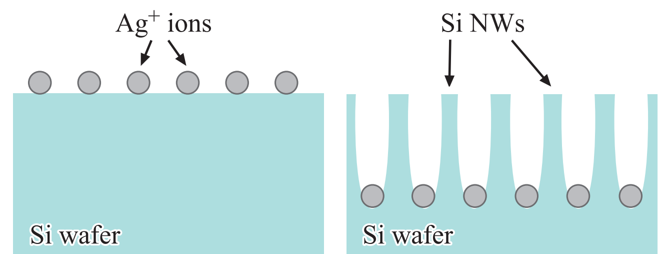

Figure 2. A schematic of the Ag^+ ions etching into the Si surface, reducing to metallic Ag0 in the process; the remaining sidewalls form the Si NWs.

of micrometers and it has been shown that Si NWs that were MAC etched using the HF/$AgNO_3$ recipe have a wide diameter distribution [29] when compared to VLS grown Si NWs [30]. The cores of these Si NWs can be single crystalline with the growth direction having a defined relationship with the surface orientation of the Si piece used [31].

The cathodic reaction for Ag^+ reduction and anodic reaction for Si oxidation are as follows (Fig. 1) [32]:

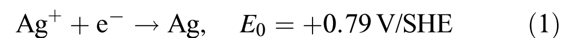

$$Ag^+ + e^- \rightarrow Ag, \quad E_0 = +0.79\,\text{V/SHE} \tag{1}$$

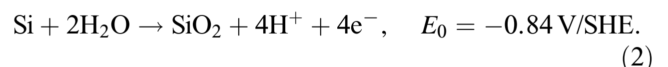

$$Si + 2H_2O \rightarrow SiO_2 + 4H^+ + 4e^-, \quad E_0 = -0.84\,\text{V/SHE}. \tag{2}$$

Si oxides are etched by HF and dissolved in aqueous solution:

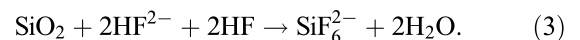

$$SiO_2 + 2HF^{2-} + 2HF \rightarrow SiF_6^{2-} + 2H_2O. \tag{3}$$

The etching mechanism proposed by Peng et al. [33] begins with the electroless deposition of Ag particles on the Si substrate. This occurs via two simultaneous electrochemical processes on the Si surface. Firstly, Ag^+ ions close to the surface of the Si capture electrons from the valence band of the Si and are deposited in the form of Ag nuclei. Secondly, the Si directly beneath the deposited metal particles, is oxidized and forms the Si hexafluoride anion (SiF_6^{2-}) which is soluble in HF. Then the metal particles (Ag^+ ions) etch through the Si and the remaining side walls form the Si

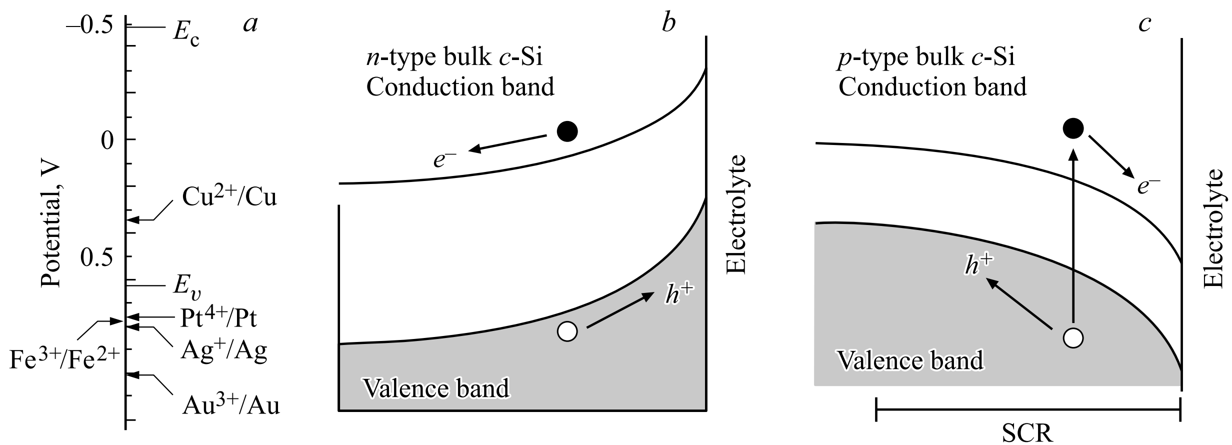

Figure 3. *a* — Qualitative diagram of the comparison between the electrochemical electron energy levels of the Si band edges (E_c and E_v are the conduction and valence band energies, respectively) and Ag^+/Ag as well as four other redox systems in HF solution; *b, c* — band bending and the motion of electrons (e^-) and holes (h^+) under the influence of the space charge region (SCR); the bands bend (*b*) upward in *n*-type Si and (*c*) downward in *p*-type Si [38].

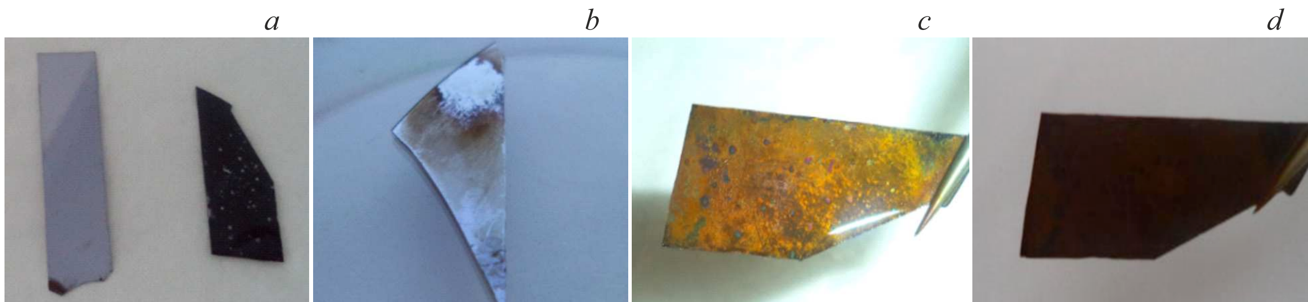

Figure 4. The prepared silicon substrates; *a* — Si before and after MAC process; *b* — Si after deposition of Cu_2O; *c, d* — Si after MAC and CBD.

NWs as shown in Fig. 2. It is generally believed that metal nanoparticles (NPs) adhered on a Si surface with a higher electronegativity and Si can attract electrons from the metal to become negatively charged (Fig. 3, *a*).

These metal NPs could then act as local micro-cathodes and enhance the cathodic reaction as a result of their catalytic activity [34,35]. It has been shown that Ag has a superior etching performance over other elements (Au, Pt, Cu or Fe) [36]. Accumulation of holes at the Si surface occurs under anodic bias and accumulation of electrons at the Si surface under cathodic bias. In the absence of a bias, band bending in the space charge region (SCR) [37], as shown in Fig. 3, pushes holes to the surface of *n*-type Si, whereas it pushes electrons to the surface of *p*-type Si. Schematics of the band diagrams at the Si-electrolyte interface are shown in Figs 3, *b* and *c*. These schematics also illustrate the difference in the work function between the *n*-type Si and *p*-type Si with reference to the electrolyte [38].

The deposited NPs covered the middle to upper segments of the Si NWs almost continuously. Thus, 20 deposition cycles were adopted in the fabrication process to obtain suitable radial NW array structures without excessive accumulation on the tops (Fig. 4, *a–d*). The cross-sectional view and top view AFM images of the as-prepared Si NWs are shown in Fig. 5. It can be seen that a high density of Si NWs, with an average height of $\sim 2.57\,\mu$m, formed vertically on the Si piece substrates.

Raman spectra of Si NWs before and after annealing are presented in Fig. 6. It shows the presence of the characteristic bands of silicon located at 519 and 309 cm^{-1}. Raman spectra reveal also the presence of Cu_2O bands at 158, 285 and 620 cm^{-1} which confirms that the Cu_2O nanoparticles are successfully deposited on the Si NWs.

From TAUC law ($\alpha h\nu = K(h\nu - Eg)^m$, with $\alpha = 2.303\,A/d$ coefficient of absorbance and $m =$ constanttake 1/2 for direct band gap and 2 for indirect band gap). This calculation gives a band gap of the overlapped bands (Si and Cu_2O) around 2.4 eV.

The PEC is formed by three electrode cell system. The working electrode consisted of the prepared sample (Cu_2O/Si NWs) while the counter and reference electrodes consisted of a Pt wire coil and SCE, respectively. The PEC was conducted in 1.0 M NaOH aqueous solution under AM

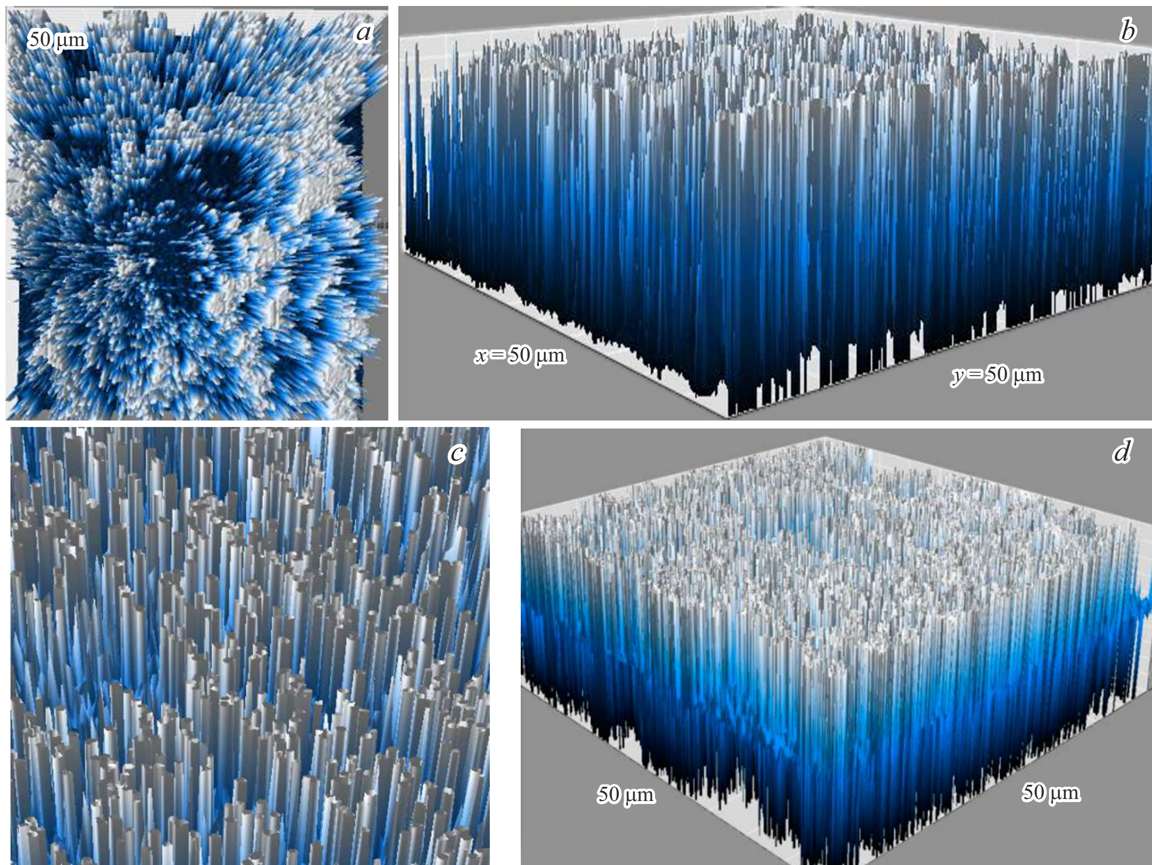

Figure 5. *a* and *b* — show the cross-sectional view and top view AFM images of the as-prepared Si NWs respectively; it can be seen that a high density of Si NWs, with an average height of $\sim 2.57\,\mu$m, formed vertically on the Si piece substrates; a typical diameter distribution of Si NWs is shown in the inset of Fig. 5, *b, c* and *d*.

1.5 illumination of 100 mW/cm^2; Figs 9, *a* and *b* — show photo current with step of 10 mV/s, in dark and in light environment.

Fig. 8, *a* shows that the measured current of bare Si NWs is very low with a maximum value of 0.008 mA/cm^2. These low current values are observed for both dark and light

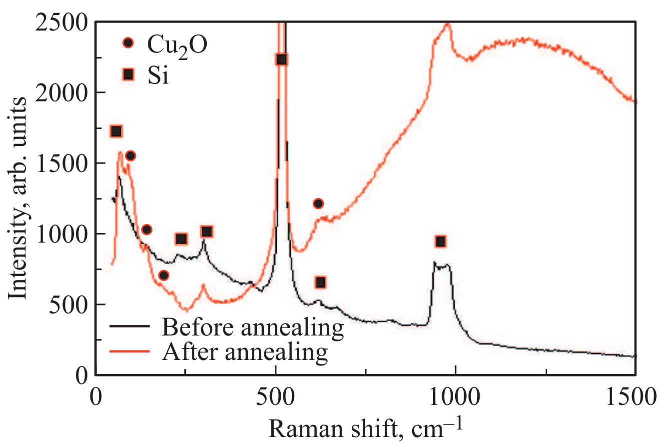

Figure 6. Raman spectra of Si NWs doped with Cu_2O nanoparticles.

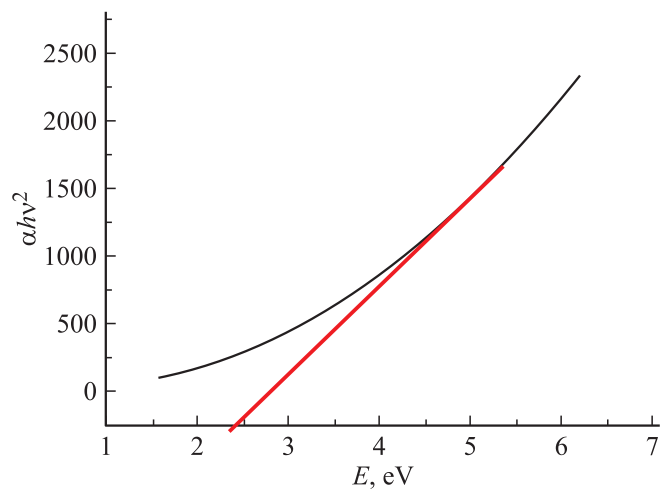

Figure 7. Graphical calculation for the band gap with the Tauc law.

environments. After Cu_2O deposition the current densities are increasing drastically compared to the bare Si NWs; it is enhanced to 13 mA/cm^2 because of the generated electrons from the heterojunction and the high specific surface area

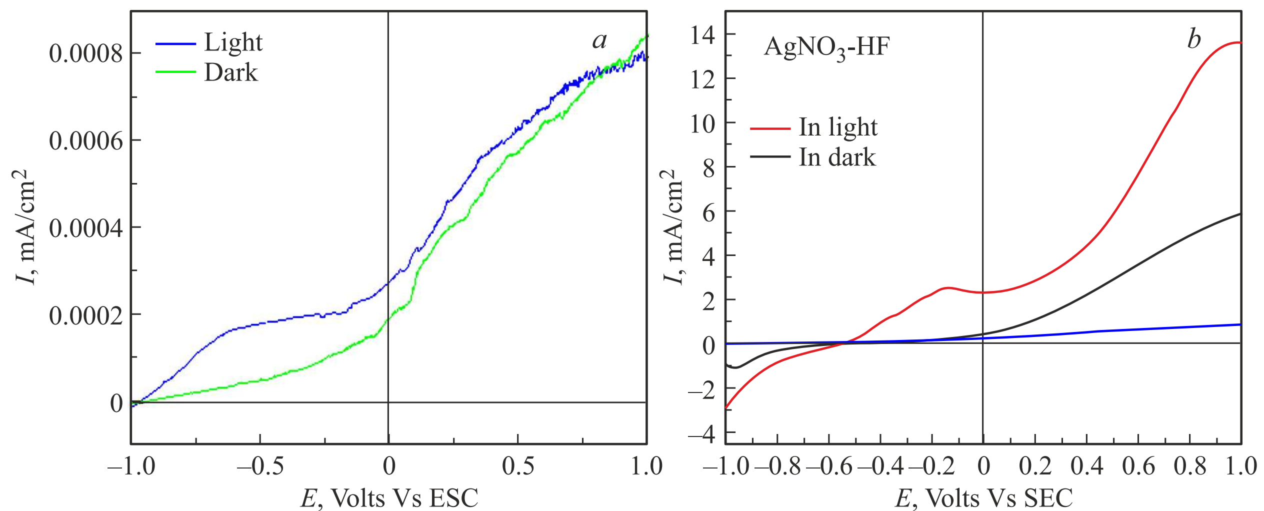

Figure 8. $I-V$ characterization in a dark and light environment *a*) of bare Si NWs and *b*) Si NW with Cu_2O.

of the nanostructures. After light exposure more electrons are collected and high current is measured ($13\,mA/cm^2$). This increasing is due to the mobility of electron trigger by light.

4. Conclusion

In conclusion, in this paper we tried to present a simple method for SiNWs/Cu_2O heterojunction fabrication. Si radial NWs are synthesized by metal assisted chemical etching method. These nanowires are observed by using AFM technique. They are immersed in a chemical bath to deposit Cu_2O semiconductor and thus SiNWs/Cu_2O heterojuncton. Raman spectroscopy confirms the presence of the Cu_2O structure by observing their characteristic peaks. The resulted structure shows a significant enhancement in the photocurrent because of specific area and also the deposition of copper oxide Cu_2O.

Competing interests

No funds, grants, or other support was received.

References

[1] S. Barth, F. Hernandez-Ramirez, J.D. Holmes, A. Romano-Rodriguez. Progr. Mater. Sci., **55**, 563 (2010).
[2] S. Chattopadhyay, L.C. Chen, K.H. Chen, NPG. Asia. Mater., **3**, 74 (2011).
[3] Z.Y. Zhang, R.J. Zou, L. Yu, J.Q. Hu. Crit. Rev. Solid State Mater. Sci., **36**, 148 (2011).
[4] K.Q. Peng, S.T. Lee. Adv. Mater., **23**, 198 (2011).
[5] B.Z. Tian, X.L. Zheng, T.J. Kempa, Y. Fang, N.F. Yu, G.H. Yu, J.L. Huang, C.M. Lieber. Nature, **449**, 885 (2007).
[6] T. Yang, H. Wang, X.M. Ou, C.S. Lee, X.H. Zhang. Adv. Mater., **24**, 6199 (2012).
[7] J.S. Li, H.Y. Yu, Y.L. Li. Nanoscale, **3**, 4888 (2011).
[8] M.D. Kelzenberg, S.W. Boettcher, J.A. Petykiewicz, D.B. Turner-Evans, M.C. Putnam, E.L. Warren, J.M. Spurgeon, R.M. Briggs, N.S. Lewis, H.A. Atwater. Nature Materials, **9**, 239 (2010).
[9] K.Q. Peng, Y. Xu, Y. Wu, Y.J. Yan, S.T. Lee, J. Zhu. Small, **1**, 1062 (2005).
[10] X. Wang, K.L. Pey, C.H. Yip, E.A. Fitzgerald, D.A. Antoniadis. J. Appl. Phys., **108**, 124303 (2010).
[11] D.W. Zenc, K.C. Yung, C.S. Xie. Scr. Mater., **44**, 2747 (2001).
[12] J.T. Zhang, J.F. Liu, Q. Peng, X. Wang, Y.D. Li. Chem. Mater., **18**, 867 (2006).
[13] H.W. Zhang, X. Zhang, H.Y. Li, Z.K. Qu, S. Fan, M.Y. Ji. Cryst. Growth Des., **7**, 820 (2007).
[14] C.L. Lee, K. Tsujino, Y. Kanda, S. Ikeda, M. Matsumura. J. Mater. Chem., **18**, 1015 (2008).
[15] Yumei YUE, Department of Mechanical Science and Engineering (Nagoya University, February 2012).
[16] G. Hodes. Phys. Chem. Chem. Phys., 9, 2181 (2007).
[17] U. Gangopadhyay, K.H. Kim, D. Mangalaraj, J.S. Yi. Appl. Surf. Sci., **230**, 364 (2004).
[18] T.P. Gujar, V.R. Shinde, C.D. Lokhande, R.S. Mane, S.H. Han. Appl. Surf. Sci., **250**, 161 (2005).
[19] J. Wei, J.M. Buriak, G. Siuzdak. Nature, **399**, 243 (1999).
[20] V. Lehmann, H. Foll. J. Electrochem. Soc., **137**, 653 (1990).
[21] L. Canham. App. Phys. Lett., **57**, 1046 (1990).
[22] A.I. Hochbaum, D. Gargas, Y.J. Hwang, P. Yang. Nano Lett., **9**, 3550 (2009).
[23] J.N. Chazalviel. *Porous Silicon Science and Technology* (Springer, Berlin, 1995).
[24] C.K. Chan, H. Peng, G. Liu, K. McIlwrath, X.F. Zhang, R.A. Huggins, Y. Cui. Nature Nanotechnol., **3**, 31 (2008).
[25] T. Tsirlina, S. Cohen, H. Cohen, L. Sapir, M. Peisach, R. Tenne, A. Matthaeus, S. Tiefenbacher, W. Jaegermann, E. Ponomarev. Sol. Energy Mater. Solar Cells, **44**, 457 (1996).
[26] M.P. Stewart, J.M. Buriak. Adv. Mater., **12**, 859 (2000).
[27] Z. Huang, N. Geyer, P. Werner, J. De Boor, U. Gösele. Adv. Mater., **23**, 285 (2011).
[28] Z. Xing, Z. Ju, J. Yang, H. Xu, Y. Qian. Nano Res., **5**, 477 (2012).

[29] N. Megouda, T. Hadjersi, G.O. Piret, R. Boukherroub, O. Elkechai. Appl. Surf. Sci., **255**, 6210 (2009). DOI: 10.1016/j.apsusc.2009.01.075
[30] J. Lim, K. Hippalgaonkar, S.C. Andrews, A. Majumdar, P. Yang. Nano Lett., **12**, 2475 (2012).
[31] M.L. Zhang, K.Q. Peng, X. Fan, J.S. Jie, R.Q. Zhang, S.T. Lee, N.B. Wong. J. Phys. Chem. C, **112**, 4444 (2008).
[32] K. Peng, H. Fang, J. Hu, Y. Wu, J. Zhu, Y. Yan, S. Lee. Chem a. Europ. J., **12**, 7942 (2006).
[33] W.D. Callister, D.G. Rethwisch. *Fundamentals of materials science and engineering: an integrated approach* (John Wiley & Sons, 2012).
[34] I. Teerlinck, P. Mertens, H. Schmidt, M. Meuris, M. Heyns. J. Electrochem. Soc., **143**, 3323 (1996).
[35] P. Gorostiza, R. Díaz, J. Servat, F. Sanz, J.R. Morante. J. Electrochem. Soc., **144**, 909 (1997).
[36] J. Kim, H. Han, Y.H. Kim, S.H. Choi, J.C. Kim, W. Lee. ACS Nano, **5**, 3222 (2011).
[37] Z. Li, L. Zhao, H. Diao, C. Zhou, H. Li, W. Wang. Int. J. Electrochem. Sci., **8**, 1163 (2013).
[38] B. Conway. *Electrochemical supercapacitors: scientific fundamentals and technologicalapplications (POD)* (Kluwer Academic/plenum, N.Y., 1999).